

# Scanning transmission X-ray microscopy probe for *in situ* mechanism study of graphene-oxide-based resistive random access memory

Hyun Woo Nho,<sup>a,‡</sup> Jong Yun Kim,<sup>a,b,‡</sup> Jian Wang,<sup>c</sup> Hyun-Joon Shin,<sup>d</sup>  
Sung-Yool Choi<sup>b</sup> and Tae Hyun Yoon<sup>a,\*</sup>

<sup>a</sup>Department of Chemistry, Hanyang University, 222 Wangsimniro, Seoul 133-791, Republic of Korea, <sup>b</sup>Department of Electrical Engineering and Graphene Research Center, KAIST, 291 Daehak-ro, Daejeon 305-701, Republic of Korea, <sup>c</sup>Canadian Light Source Inc., University of Saskatchewan, 44 Innovation Boulevard, Saskatoon, Saskatchewan, Canada S7N 2V3, and <sup>d</sup>Pohang Accelerator Laboratory and Department of Physics, Pohang University of Science and Technology, 80 Jigokro-127-beongil, Pohang, Gyeongbuk 790-834, Republic of Korea. \*E-mail: thyoon@gmail.com

Here, an *in situ* probe for scanning transmission X-ray microscopy (STXM) has been developed and applied to the study of the bipolar resistive switching (BRS) mechanism in an Al/graphene oxide (GO)/Al resistive random access memory (RRAM) device. To perform *in situ* STXM studies at the C *K*- and O *K*-edges, both the RRAM junctions and the  $I_0$  junction were fabricated on a single  $\text{Si}_3\text{N}_4$  membrane to obtain local XANES spectra at these absorption edges with more delicate  $I_0$  normalization. Using this probe combined with the synchrotron-based STXM technique, it was possible to observe unique chemical changes involved in the BRS process of the Al/GO/Al RRAM device. Reversible oxidation and reduction of GO induced by the externally applied bias voltages were observed at the O *K*-edge XANES feature located at 538.2 eV, which strongly supported the oxygen ion drift model that was recently proposed from *ex situ* transmission electron microscope studies.

**Keywords:** *in situ*; scanning transmission X-ray microscopy; STXM; graphene oxide; GO-RRAM; bipolar resistive switching mechanism; oxygen ion drift model.

© 2014 International Union of Crystallography

## 1. Introduction

Scanning transmission X-ray microscopy (STXM) is a novel spectromicroscopic technique that typically uses finely focused soft X-rays from a highly brilliant third-generation synchrotron source. Owing to recent developments in X-ray optics and the extended availability of third-generation synchrotron sources, this novel analytical technique has become an important tool for the analysis of complex specimens in a number of scientific disciplines, including chemistry (Jeong *et al.*, 2008), biology (Benzerara *et al.*, 2008; Leung *et al.*, 2009), material science (Najafi *et al.*, 2010; Zhou *et al.*, 2010*a,b*; Pacilé *et al.*, 2011) and environmental sciences (Lam *et al.*, 2010; Yoon *et al.*, 2006; Benzerara *et al.*, 2005). The development of X-ray focusing optics (*e.g.* Fresnel-zone-plate lens) to a diffraction-limited spot enabled spatial resolution of this technique down to a few tens of nanometers (Takekoh *et al.*, 2005; Chao *et al.*, 2012), while an increasing number of STXM beamlines are available for the general user community, including the ALS (beamlines 5.3.2 and 11.0.2), BESSY II

(U41), NSLS (X1A), CLS (SM beamline), SLS (PolLux) and PLS (10A), and several others are in planning, construction or commissioning stages (Kilcoyne *et al.*, 2003; Nilsson *et al.*, 2005; Karunakaran, 2009; Hitchcock *et al.*, 2008; Shin, 2013). Consequently, STXM is now considered as one of the most unique and powerful synchrotron-based analytical tools, providing nanometer-scale chemical information under *in situ* conditions (Yoon, 2009).

In particular, STXM has demonstrated huge potential applications in the area of material science and as an *in situ* imaging tool for monitoring chemical reactions, since quantitative knowledge on the nanoscale chemical heterogeneity is playing a key role in understanding the properties and behaviors of composite materials and related electronic devices such as carbon nanotubes, solar cells and light emitting diodes (Hub *et al.*, 2010; Smit *et al.*, 2009; Zhou *et al.*, 2011; Pacilé *et al.*, 2008; Felten *et al.*, 2006, 2007, 2010; McNeill *et al.*, 2006*a,b*, 2007, 2009). Drake *et al.* (2004) designed a microreactor-type STXM cell having Al resistive heater and microflow channels for *in situ* monitoring of redox reactions with Cu powders as catalyst. Also, Guay *et al.* (2005) performed *in situ* measure-

‡ These authors contributed equally to this work.

ments of electrochemical reactions using STXM and their homemade electrochemical wet cell for monitoring of chemical changes of polyaniline film by the applied potential.

In addition to the above advantages as an *in situ* chemical imaging tool, STXM could be further applied to *in situ* studies of various electronic devices under their operating conditions, such as a resistive random access memory (RRAM) device. Although its key operating mechanisms are not yet fully understood, owing to its simple structure, facile processing, high density and fast switching characteristics, RRAM has attracted great attention as a promising next-generation non-volatile memory. Based on *ex situ* studies on a  $\text{TiO}_2$ -RRAM device, it has been postulated that the oxygen ions from an insulating interface layer ( $\text{AlO}_x$ ) diffuse into the active layer region during the ‘ON’ state of the device (Jeong *et al.*, 2009, 2010). Recently, Strachan *et al.* (2010, 2011) used STXM for the study of local conducting channel formation in a  $\text{TiO}_2$ -RRAM device. They observed subtle changes at Ti *L*-edge absorption spectra in Pt/ $\text{TiO}_2$ /Pt RRAM that confirmed the origin of the bipolar resistance switching (BRS) mechanism as this local reduction of  $\text{TiO}_2$  to metallic  $\text{Ti}_4\text{O}_7$ .

Currently, among the materials used as an active layer of the RRAM device, graphene oxide (GO) is considered as one of the most promising candidates, due to its unique advantages such as transparency, flexibility, low cost of fabrication, low-power consumption and fast switching speed (He *et al.*, 2009). We have also performed *ex situ* studies on a GO-RRAM device using high-resolution transmission electron microscopy to elucidate the BRS mechanism in a GO-based RRAM system and have suggested that oxidation/reduction phenomena are involved in this GO-based flexible non-volatile memory (Jeong *et al.*, 2010). However, in the case of the GO-RRAM device, there might be more than simple ‘oxidation/reduction’ reactions involved in its BRS mechanism, such as local chemical changes of GO functional groups (*e.g.* hydroxyl, ketone, ester and carboxylate), which cannot be probed by current TEM-EELS approaches and need to be further probed by STXM with C and O *K*-edge XANES spectroscopy. In contrast to the STXM studies at the Ti *L*-edge having linear baseline/background, C and O *K*-edge studies need more delicate  $I_0$  measurements and spectral processing. Due to the linear background of XANES at the Ti *L*-edge, inverted transmission spectra are similar to their optical density (OD) spectra, so XANES spectra of the Ti *L*-edge can be measured without the  $I_0$  region. However, acquisition of C and O *K*-edge XANES spectra is much more complicated than for the Ti *L*-edge. A significantly distorted OD can originate by inaccurate  $I_0$ . Therefore a way to make a blank region free of spin-coated GO in the same device was inevitably required. We have successfully developed and fabricated an  $I_0$  region in the device by the partial etching process using  $\text{O}_2$  plasma treatment and a shadow mask. Additionally, since all STXM measurements should be performed in ‘transmission’ mode and require a very thin sample with appropriate OD ranges (0.3–0.8), a typical RRAM memory device with thick silicon substrate cannot be directly tested in STXM. To overcome this restriction, we have designed and fabricated a special STXM

probe for *in situ* studies of operating mechanisms in a GO-RRAM device. Using this probe combined with the synchrotron-based STXM technique, we were able to observe unique chemical changes involved in the BRS process of the Al/GO/Al RRAM device. Moreover, in addition to this application for the RRAM device, these unique characteristics of STXM are expected to benefit studies on the operating mechanisms of thin film devices with buried interfaces, such as solar cells and light emitting diodes.

## 2. Experimental

### 2.1. Fabrication of GO-RRAM on $\text{Si}_3\text{N}_4$ membrane for STXM measurements

The RRAM device for *in situ* STXM measurements is comprised of (i) a printed circuit board (PCB) sample holder equipped with two subminiature-C (SMC) type electrical connectors and Cu electrodes, and (ii) a  $\text{Si}_3\text{N}_4$  membrane with the RRAM device, as shown in Fig. 1(a). The physical dimensions of the PCB-based sample holder are the same as for a typical STXM sample holder. The thickness of the PCB is approximately 0.8 mm and the lengths of the parallel sides are 33 mm and 19.2 mm. The height of the plate is 51 mm and the two square holes for X-ray transmission are 4 mm × 4 mm. Two Cu electrodes of width 2 mm are connected to two respective SMC connectors.

The structure of the RRAM device used in this study is represented in Figs. 1(b) and 1(c). It was specially fabricated on a purchased  $\text{Si}_3\text{N}_4$  membrane (NX7150D, Norcada, Canada; 1.5 mm × 1.5 mm window membrane with 200 nm thickness). The RRAM device has top and bottom Al electrodes with approximately 30 nm thickness, and the GO active layer of a few nanometers thickness is sandwiched between

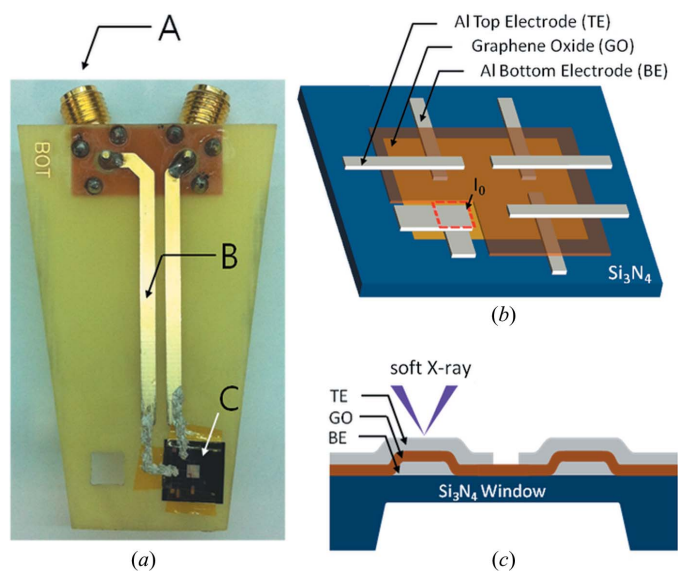


**Figure 1** (a) Photograph of the electrochemical *in situ* sample holder: A is a SMC connector, B is a Cu electrode, and C is a mounted RRAM. (b) Structural schematic diagram of the GO-RRAM. (c) Cross-sectional view of the RRAM.

these two electrodes. The detailed fabrication procedures are as follows. Firstly, a thermal evaporation technique was used to fabricate the Al bottom electrodes (BE, 40  $\mu\text{m}$  wide and 30 nm thick) on the  $\text{Si}_3\text{N}_4$  membrane with a square bar patterned shadow mask. Then GO was spin-coated on the BE/ $\text{Si}_3\text{N}_4$  at 2000 r.p.m. for 40 s. To fabricate the  $I_0$  region without GO, oxygen plasma etching was performed. A square patterned shadow mask was used to cover the GO/BE/ $\text{Si}_3\text{N}_4$ . The uncovered region (blank area in the shadow mask) was etched by  $\text{O}_2$  plasma for 30 s at 50 W with a 60  $\text{cm}^3 \text{min}^{-1}$  flow rate of oxygen gas. Finally, the Al top electrode (TE, 40  $\mu\text{m}$  wide and 30 nm thick) was deposited on the GO/BE/ $\text{Si}_3\text{N}_4$  by thermal evaporation method. The fabricated TE and BE were perpendicular to each other. The RRAM device on the  $\text{Si}_3\text{N}_4$  membrane was mounted on the hole of the PCB sample holder and TE and BE were connected to respective Cu electrodes with Ag paste, while the Cu electrodes were connected to the SMC-type electrical connectors by Pb soldering, as shown in Fig. 1(a).

2.2. *In situ* STXM experimental set-up for RRAM

A schematic illustration of the *in situ* STXM set-up for the RRAM device is presented in Fig. 2. The monochromatic soft X-rays of the synchrotron source were focused onto a fine spot (e.g. spot size of 30–50 nm full width at half-maximum) by a Fresnel zone plate (ZP), a circular diffraction grating consisting of a series of patterned Au rings on a transparent  $\text{Si}_3\text{N}_4$  window. In this study we used a ZP with an outermost zone width of 25 nm. An order-sorting aperture (OSA) was used to block the undesired diffraction orders (more than first

order) of X-rays from the zone plate. The intensity of the transmitted X-rays was measured by scintillator PMT detector. Samples were raster scanned by a piezoelectric stage in the  $x$  and  $y$  directions for fine scanning or stepper motor stages for coarse scanning. The piezoelectric stage was mounted on the stepper motor stages. For precision, the same area of sample was scanned repetitively at different X-ray energies *via* interferometrically controlled stages; therefore, not only images at a single photon energy but also stacks (a sequence of images taken at the same region of interest) at various photon energies could be acquired. The STXM chamber was filled with He to minimize thermal drift of the stages. *aXis2000* software was used to process the image stacks and extract XANES spectra (Hitchcock, 2012).

The RRAM sample mounted on the *in situ* sample holder was connected to a sourcemeter (Keithley 2400) to apply voltage and measure current. The  $I$ - $V$  curve was measured by voltage sweep from  $-4$  V to  $+3$  V, and the voltage sweep was turned off before collecting stack images at the ‘OFF’ state of  $-1.5$  V and ‘ON’ state of the same voltage. C and O  $K$ -edge XANES were acquired by two region stacks to investigate the changes of the functional groups in the GO film used as the active layer of RRAM. It took about one hour for acquisition of a two-region stack for a junction of electrodes of  $50 \mu\text{m} \times 50 \mu\text{m}$  and a blank region of  $20 \mu\text{m} \times 20 \mu\text{m}$ . As the measurement time was not too long, the drift was below  $1 \mu\text{m}$ , and it could also be aligned by using the ‘align stack’ function of *stack-analyze* (Jacobsen, 2009). Therefore the drift of imaging might have little influence on the results. It is important to perform non-destructive *in situ* measurements of samples to compare the changes induced by the external

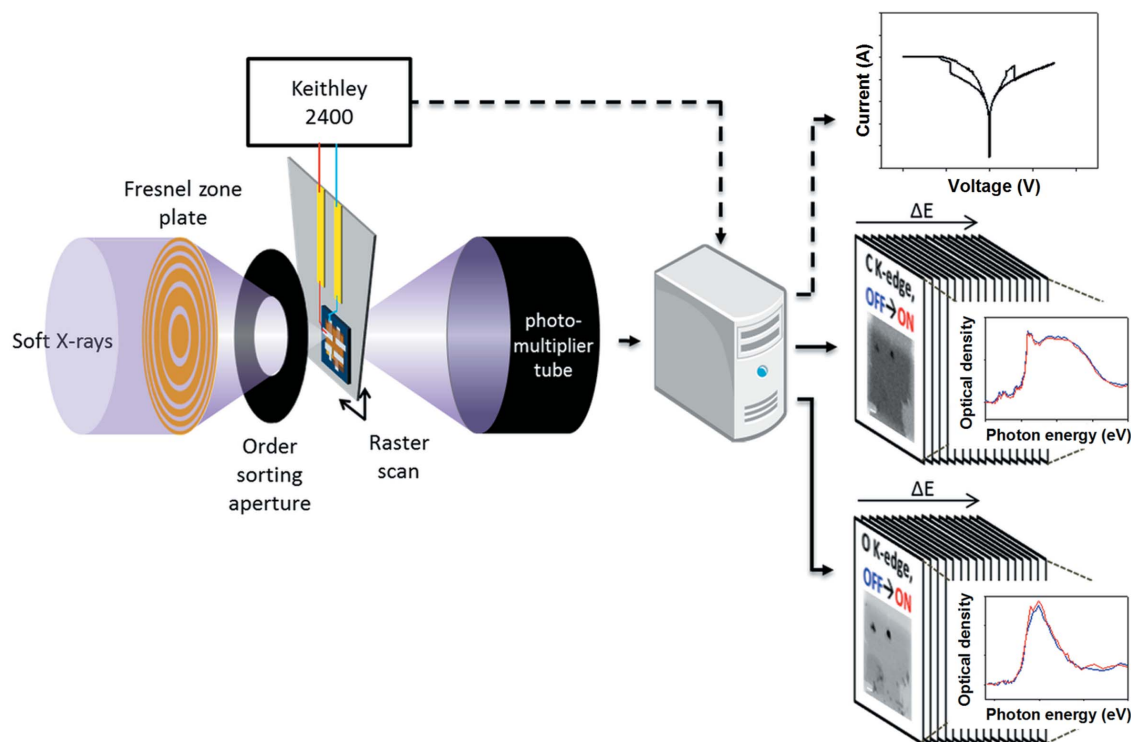


Figure 2 Schematic diagram of STXM measurement for the study of the GO-RRAM operating mechanism.

stimulus. In the case of thin film samples such as GO-RRAM, intra-sample heterogeneity would be easily generated by small variations in thickness or chemical inhomogeneity of samples, resulting in significant alteration of signals. Also, it is difficult to recognize subtle differences in very thin samples with low signal-to-noise ratio. Therefore, it is essential to characterize the synchronized variations induced by the periodic external stimulus in an identical sample under *in situ* conditions.

### 3. Results and discussion

As illustrated in Fig. 1(b), three RRAM junctions and one  $I_0$  junction were fabricated on top of the  $\text{Si}_3\text{N}_4$  window and STXM measurements at the C and O  $K$ -edges were performed for these RRAM junctions as well as the  $I_0$  junction. Fig. 3(a) shows a C  $K$ -edge STXM image of a  $600\ \mu\text{m} \times 600\ \mu\text{m}$  area including one of the RRAM junctions (region A) and the  $I_0$  junction (region B). As shown in this image, different regions of the device (*e.g.* TE, BE, RRAM junction,  $I_0$  region) can be clearly distinguished. It is different from  $\text{TiO}_2$ -based RRAM having a linear background; the  $I_0$  region within the measured sample is essential for GO-RRAM to acquire accurate XANES spectra of C and O  $K$ -edges by STXM. Without a proper  $I_0$  region, the transmitted X-rays cannot be converted to OD, and the subtle transitions cannot be identified. Therefore, fabrication of a blank region without GO is critical

for GO-RRAM. In particular, in the vicinity of the  $I_0$  junction area, several regions with different layers of Al electrodes were observed, which could be used as  $I_0$  for the GO-associated TE, BE and RRAM junction. For instance, region B ( $I_0$  junction) is composed of two layers of Al electrodes (BE and TE) without GO, while region C contains only one layer of Al electrode (BE) on top of the bare  $\text{Si}_3\text{N}_4$  membrane and region D contains bare  $\text{Si}_3\text{N}_4$  membrane with no Al electrode. Therefore, regions B, C and D could be used as  $I_0$  for the junction of RRAM, TE/GO and GO/BE regions, respectively. For the RRAM junction area [region A in Fig. 3(a)], optical and STXM [at 292.0 eV (C  $K$ -edge) and 538.2 eV (O  $K$ -edge)] images were also obtained with higher magnification and are presented in Figs. 3(b)–3(d). Interestingly, several similarities and differences were observed between these optical and STXM images of the RRAM junction. For example, the darkest spots shown in Fig. 3(d) (regions E and F) were also observed in the optical image by reflection mode (Fig. 3b), indicating surface contamination or irregularities in these regions. However, slightly darker regions G, H and I observed in Fig. 3(d) were not observed in both the optical image (Fig. 3b) and the STXM image at the C  $K$ -edge (Fig. 3c) which suggests that those slightly darker regions originated from heterogeneities of the varied layers rather than surface irregularities of the TE.

As presented in Fig. 4(a), the  $I$ - $V$  curves measured for the Al/GO/Al RRAM device on  $\text{Si}_3\text{N}_4$  membrane displayed typical bipolar resistive switching characteristics. The  $I$ - $V$  curve shown in Fig. 4(a) displays sudden decreases in resistance (increase in current level) at  $-2\ \text{V}$  and abrupt increases in resistance (decrease in current level) at  $+1.5\ \text{V}$ . STXM image stacks were also acquired during these  $I$ - $V$  curve measurements with the sweep voltage ranging from  $-4$  to  $+3\ \text{V}$ . The bias was first scanned from 0 to  $-1.5\ \text{V}$  and a STXM image stack at the O  $K$ -edge was acquired under this 'OFF' state. Then, the voltage bias was further scanned down to  $-4\ \text{V}$  to turn the device into the 'ON' state and returned to  $-1.5\ \text{V}$  for the second STXM stack measurement. After that, the voltage bias was further swept to complete the cycle:  $-1.5\ \text{V} \rightarrow 0\ \text{V} \rightarrow +4\ \text{V} \rightarrow 0\ \text{V}$ . These *in situ* acquisitions of the STXM image stacks during the  $I$ - $V$  curve measurement cycles were repeated several times to confirm the observed changes in XANES spectra [see Figs. 4(b) and 4(c), and Figs. S1(a) and S1(b) of the supporting information<sup>1</sup>]. For the 'ON' and 'OFF' states of the first two cycles, STXM image stacks were processed and O  $K$ -edge XANES spectra were obtained from various regions of the junction [regions E, F, G and H in Fig. 3(d)]. These O  $K$ -edge XANES spectra, displayed in Figs. 4(b) and 4(c) and Figs. S1(a) and S1(b), have a main peak at 540.2 eV with a shoulder peak located at 538 eV. Interestingly, slight but still evident changes were repeatedly observed in the O  $K$ -edge XANES spectra from the regions G and H [shown in Figs. 4(b) and 4(c)], while no observable changes in the O  $K$ -edge XANES spectra were found in the regions

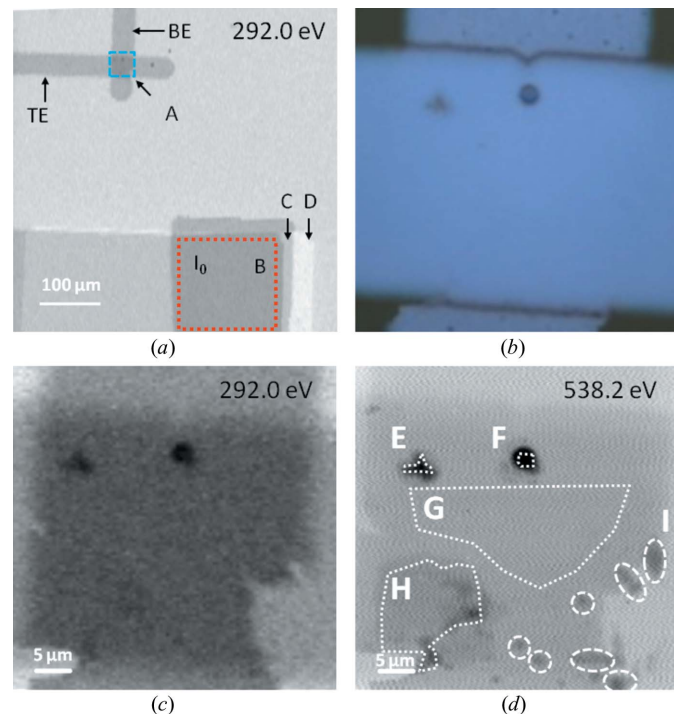


**Figure 3**

(a) STXM transmission image of the RRAM junction region (marked by a blue dashed box) and  $I_0$  (marked by a red short-dashed box) at low magnification, taken at 292.0 eV. The bottom and top electrodes are labeled as BE and TE. (b) Optical microscopic image of region A. (c, d) STXM transmission images of region A at 292.0 eV (c) and 538.2 eV (d). The damaged area at the bottom right-hand side of the RRAM junction region [shown in (c) and (d)] was due to the shadow mask which was partially blocked by debris.

<sup>1</sup> Supporting information for this paper is available from the IUCr electronic archives (Reference: RV5007).

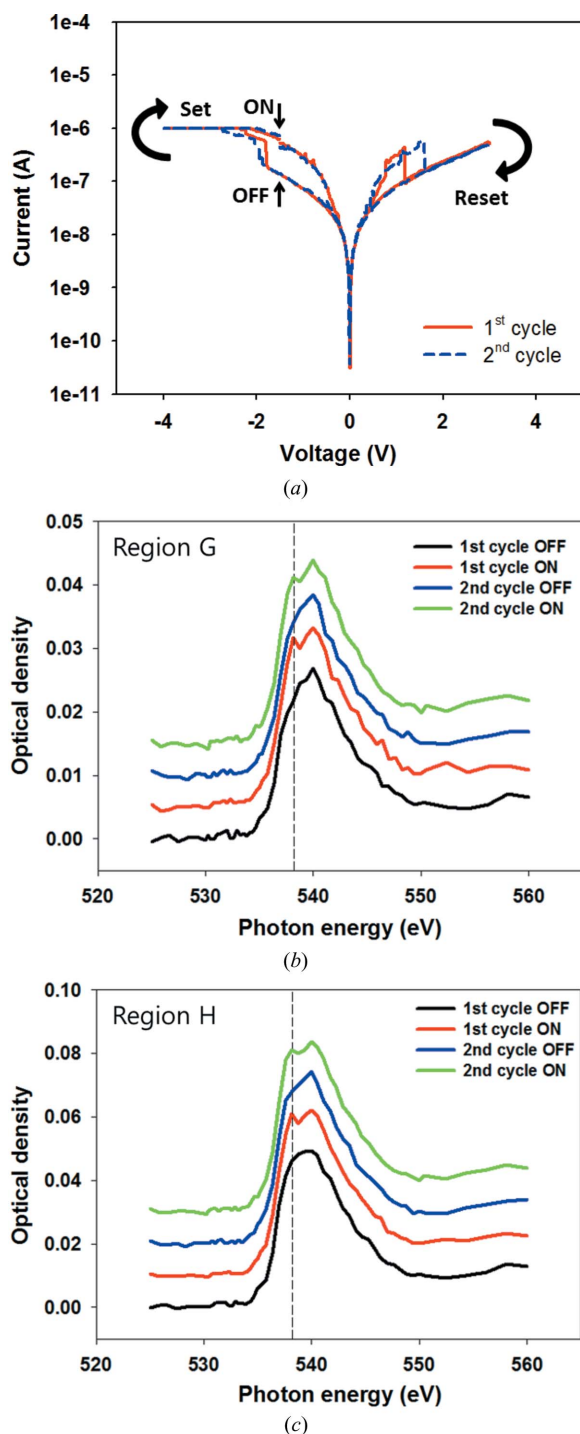


**Figure 4** (a) *I*-*V* curve. (b)–(c) O *K*-edge XANES spectra of RRAM in region *G* (b) and region *H* (c).

*E* and *F* (shown in Fig. S1). Another difference between these regions was that the OD of regions *G* and *H* was much lower than that of regions *E* and *F*, which suggests that the dark spot regions *E* and *F* were much thicker or highly oxidized than the surrounding regions *G* and *H*, based on the Beer–Lambert law. The absence of observable O *K*-edge XANES spectral changes in the regions *E* and *F* can be ascribed to contamination or the irregularity in film thickness, since the stronger

spectral signal from the thick oxide layers may mask the weak spectral changes originating from the interfacial oxidation/reduction process at the TE/GO interface. Therefore, significant and reproducible changes in the O *K*-edge XANES spectra were observed only in the regions *G* and *H* with thinner GO film without contamination.

As shown in Figs. 4(b) and 4(c), during the switching cycles between the ‘OFF’ and ‘ON’ states of the RRAM device, enhancement in the peak at 538.2 eV was repeatedly observed in the regions *G* and *H*. This peak at 538.2 eV could be assigned to O  $1s \rightarrow \sigma^*$  transitions of C=O or C–O bonds (Yang & Hu, 2012; Lee *et al.*, 2010; Kim *et al.*, 2011; Zelenay *et al.*, 2011). The spectral changes induced by the external bias can be attributed to the chemical changes in the GO active layer of the RRAM. When the interfacial oxides of TE are reduced by applying negative bias, the oxygen ions will diffuse into the GO active layer, and cause further oxidation of the GO active layer, such as hydroxyl, epoxy, carboxyl or ketone groups, with corresponding peaks located at 538.2 eV. The oxidation of GO and reduction of the interfacial aluminium oxide layer creates the ‘ON’ state RRAM with low resistance. On the other hand, under the positive bias, when the oxygen ions from the hydroxyl, carboxyl or ketone groups of the GO layer diffuse back to the top interfacial Al oxide layer, the insulating layer (interfacial oxide layer) will become thicker, and the RRAM turns into the ‘OFF’ state with high resistance. This reversible oxidation and reduction of GO by the external bias was represented by reproducible changes of the peak at 538.2 eV as shown in Figs. 4(b) and 4(c). Previously, it has been reported that the GO can be reversibly reduced or oxidized under an applied bias between –2.5 V and 2.5 V (Ekiz *et al.*, 2011). Thus, based on our *in situ* STXM observations, we propose that the BRS mechanism in this GO RRAM device can be ascribed to the redox reaction between GO and the AlO<sub>x</sub> barrier layer. Although further C *K*-edge STXM studies to clarify more explicitly the functional groups responsible for these phenomena are still in progress, we believe that the observed changes in O *K*-edge XANES spectra at 538.2 eV strongly support the oxygen ion drift model for resistance changes in GO-RRAM, as we recently proposed from *ex situ* TEM studies (Jeong *et al.*, 2010). Additionally, repeatedly observed changes in the O *K*-edge XANES spectra also confirmed that there were no significant damage or irreversible decomposition reactions under the given operating conditions. Under the negatively applied bias and joule heating, it has been reported that GO can be decomposed to CO<sub>2</sub>. Upon rapid heating to a temperature of 473 K, GO was known to experience exothermic decomposition reactions to produce CO<sub>2</sub> which is thermodynamically the most stable oxide form of carbon (Zuckerman & Hagen, 1990; Gilje *et al.*, 2010). Moreover, if there are any decomposition reactions of the GO layer by joule heating, the CO<sub>2</sub> gas accumulates at the GO/TE interface until its pressure becomes large enough to break through the GO/TE layer, then TE can be peeled off by the escaping CO<sub>2</sub> gas (see Fig. S2), as observed for other types of RRAM device (Strachan *et al.*, 2009). Therefore, the irreversible changes should have resulted in a thickness reduction

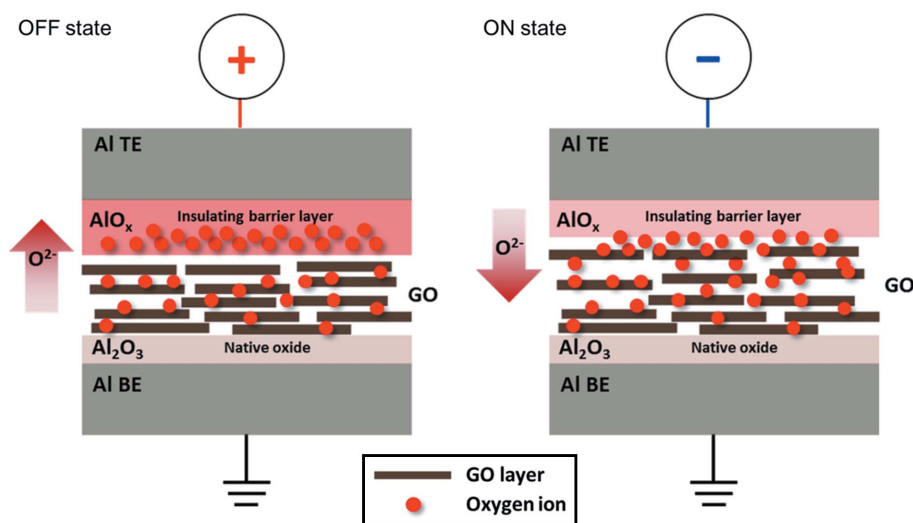


**Figure 5**  
Schematic illustration of BRS mechanisms in an Al/GO/Al RRAM device.

of the film and/or volcano-like surface structures formed during the gas escaping processes. However, we could not observe any significant OD reduction or irregular surface formation during these repeated switching processes of GO-RRAM, suggesting that the applied bias was not enough to cause any significant damage or irreversible decomposition reactions.

A schematic illustration of the BRS mechanism of the Al/GO/Al device is shown in Fig. 5. In our recent *ex situ* X-ray photoelectron spectroscopy and TEM study of the Al/GO/Al RRAM device (Jeong *et al.*, 2010), we have suggested that the interfacial oxide layer was spontaneously formed between TE and GO, and the redox reactions between this interfacial oxide layer and GO played a key role in the BRS mechanism of the RRAM device. Therefore, the RRAM device with Al electrodes showed good memory characteristics because the Al electrodes can be easily oxidized and formed an aluminium oxide layer that functioned as a reservoir of oxygen at the interface between the GO; whereas RRAM using inert metal (*e.g.* Au) electrodes did not work well because an interfacial oxide layer could not be formed between the inert metal electrodes and GO (Jeong *et al.*, 2010). In this study, by using an *in situ* STXM probe for thin film devices (*e.g.* RRAM device), we have confirmed BRS mechanisms in an Al/GO/Al RRAM device, *via in situ* observation of the reversible oxidation and reduction of GO/TE, as shown in Figs. 4(b) and 4(c).

#### 4. Conclusion

To investigate operating mechanisms of various thin film devices under *in situ* conditions, we have developed an *in situ* STXM probe and applied it to the study of BRS mechanisms in an Al/GO/Al RRAM device. To perform *in situ* spectro-microscopic studies in ‘transmission’ mode, GO-RRAM devices involving very thin films within appropriate OD ranges were fabricated on  $\text{Si}_3\text{N}_4$  membranes. Additionally, both the

RRAM junctions and the  $I_0$  junction were fabricated on a single  $\text{Si}_3\text{N}_4$  membrane for the accurate measurements of C and O *K*-edge XANES spectra, which require more delicate  $I_0$  normalization. Using this *in situ* probe combined with the synchrotron-based STXM technique, we were able to observe reversible redox reactions repeatedly occurring in an Al/GO/Al RRAM device under operating cycles. Moreover, this *in situ* STXM probe combined with unique capabilities of STXM is expected to benefit future studies on the operating mechanisms of thin film devices with buried interfaces, such as solar cells and light emitting diodes.

This research was supported by the Basic Science Research Program through the National Research Foundation of Korea (NRF) funded by the Ministry of Education (NRF-2012R1A1A2009505). HWN and HJS also appreciate support from the Korea government, Ministry of Science, ICT and Future Planning (MSIP) (No. 20080062606, CELA-NCRC) and PAL through the abroad beam time program of the Synchrotron Radiation Facility Project under MEST. SYC and JYK acknowledge grants from the Global Frontier Research Center for Advanced Soft Electronics (NRF, 20110033640) and the Creative Research Program of ETRI (13ZE1110). We also thank Dr C. Karunakaran and Y. Lu for their assistance at CLS SM beamline. The Canadian Light Source is supported by the Natural Sciences and Engineering Research Council of Canada, the National Research Council Canada, the Canadian Institutes of Health Research, the Province of Saskatchewan, Western Economic Diversification Canada, and the University of Saskatchewan.

#### References

- Benzerara, K., Morin, G., Yoon, T. H., Miot, J., Tyliszczak, T., Casiot, C., Bruneel, O., Farges, F. & Brown, G. E. Jr (2008). *Geochim. Cosmochim. Acta*, **72**, 3949–3963.
- Benzerara, K., Yoon, T. H., Menguy, N., Tyliszczak, T. & Brown, G. E. Jr (2005). *Proc. Natl Acad. Sci. USA*, **102**, 979–982.
- Chao, W., Fischer, P., Tyliszczak, T., Rekawa, S., Anderson, E. & Naulleau, P. (2012). *Opt. Express*, **20**, 9777–9783.
- Drake, I. J., Liu, T. C. N., Gilles, M., Tyliszczak, T., Kilcoyne, A. L. D., Shuh, D. K., Mathies, R. A. & Bell, A. T. (2004). *Rev. Sci. Instrum.* **75**, 3242.
- Ekiz, O. O., Ürel, M., Güner, H., Mizrak, A. K. & Dâna, A. (2011). *ACS Nano*, **5**, 2475–2482.
- Felten, A., Bittencourt, C., Pireaux, J.-J., Reichelt, M., Mayer, J., Hernandez-Cruz, D. H. & Hitchcock, A. P. (2007). *Nano Lett.* **7**, 2435–2440.
- Felten, A., Gillon, X., Gulas, M., Pireaux, J.-J., Ke, X., Tendeloo, G. V., Bittencourt, C., Najafi, E. & Hitchcock, A. P. (2010). *ACS Nano*, **4**, 4431–4436.

- Felten, A., Hody, H., Bittencourt, C., Pireaux, J.-J., Cruz, D. H. & Hitchcock, A. P. (2006). *Appl. Phys. Lett.* **89**, 093123.
- Gilje, S., Dubin, S., Badakhshan, A., Farrar, J., Danczyk, S. A. & Kaner, R. B. (2010). *Adv. Mater.* **22**, 419–423.
- Guay, D., Stewart-Ornstein, J., Zhang, X. & Hitchcock, A. P. (2005). *Anal. Chem.* **77**, 3479–3487.
- He, C. L., Zhuge, F., Zhou, X. F., Li, M., Zhou, G. C., Liu, Y. W., Wang, J. Z., Chen, B., Su, W. J., Liu, Z. P., Wu, Y. H., Cui, P. & Li, R.-W. (2009). *Appl. Phys. Lett.* **95**, 232101.
- Hitchcock, A. P. (2012). *aXis2000*, <http://unicorn.mcmaster.ca/aXis2000.html>.
- Hitchcock, A. P., Dynes, J. J., Johansson, G., Wang, J. & Botton, G. (2008). *Micron*, **39**, 311–319.
- Hub, C., Burkhardt, M., Halik, M., Tzvetkov, G. & Fink, R. (2010). *J. Mater. Chem.* **20**, 4884.
- Jacobsen, C. (2009). *stack-analyze*, <http://xray1.physics.sunysb.edu/data/software.php>.
- Jeong, H. Y., Kim, J. Y., Kim, J. W., Hwang, J. O., Kim, J. E., Lee, J. Y., Yoon, T. H., Cho, B. J., Kim, S. O., Ruoff, R. S. & Choi, S. Y. (2010). *Nano Lett.* **10**, 4381–4386.
- Jeong, H. Y., Lee, J. Y. & Choi, S.-Y. (2010). *Adv. Funct. Mater.* **20**, 3912–3917.
- Jeong, H. Y., Lee, J. Y., Choi, S.-Y. & Kim, J. W. (2009). *Appl. Phys. Lett.* **95**, 162108.
- Jeong, H.-K., Noh, H.-J., Kim, J.-Y., Jin, M. H., Park, C. Y. & Lee, Y. H. (2008). *Europhys. Lett.*, **82**, 67004.
- Karunakaran, C. (2009). CLS Science (Beamline 10ID-1). Canadian Light Source, Saskatoon, Saskatchewan, Canada.
- Kilcoyne, A. L. D., Tylliszczak, T., Steele, W. F., Fakra, S., Hitchcock, P., Franck, K., Anderson, E., Harteneck, B., Rightor, E. G., Mitchell, G. E., Hitchcock, A. P., Yang, L., Warwick, T. & Ade, H. (2003). *J. Synchrotron Rad.* **10**, 125–136.
- Kim, K., Zhu, P., Li, N., Ma, X. & Chen, Y. (2011). *Carbon*, **49**, 1745–1751.
- Lam, K. P., Hitchcock, A. P., Obst, M., Lawrence, J. R., Swerhone, G. D. W., Leppard, G. G., Tylliszczak, T., Karunakaran, C., Wang, J., Kaznatcheev, K., Bazylnski, D. A. & Lins, U. (2010). *Chem. Geol.* **270**, 110–116.
- Lee, D. W., De Los Santos, V. L., Seo, J. W., Felix, L. L., Bustamante, D. A., Cole, J. M. & Barnes, C. H. W. (2010). *J. Phys. Chem. B*, **114**, 5723–5728.
- Leung, B. O., Hitchcock, A. P., Cornelius, R., Brash, J. L., Scholl, A. & Doran, A. (2009). *Biomacromolecules*, **10**, 1838–1845.
- McNeill, C. R., Watts, B., Thomsen, L., Ade, H., Greenham, N. C. & Dastoor, P. C. (2007). *Macromolecules*, **40**, 3263–3270.
- McNeill, C. R., Watts, B., Thomsen, L., Belcher, W. J., Greenham, N. C. & Dastoor, P. C. (2006a). *Nano Lett.* **6**, 1202–1206.
- McNeill, C. R., Watts, B., Thomsen, L., Belcher, W. J., Greenham, N. C., Dastoor, P. C. & Ade, H. (2009). *Macromolecules*, **42**, 3347–3352.
- McNeill, C. R., Watts, B., Thomsen, L., Belcher, W. J., Kilcoyne, A. L. D., Greenham, N. C. & Dastoor, P. C. (2006b). *Small*, **2**, 1432–1435.
- Najafi, E., Wang, J., Hitchcock, A. P., Guan, J., Dénomée, S. & Simard, B. (2010). *J. Am. Chem. Soc.* **132**, 9020–9029.
- Nilsson, H. J., Tylliszczak, T., Wilson, R. E., Werme, L. & Shuh, D. K. (2005). *Anal. Bioanal. Chem.* **383**, 41–47.
- Pacilé, D., Meyer, J. C., Fraile Rodríguez, A. F., Papagno, M., Gómez-Navarro, C., Sundaram, R. S., Burghard, M., Kern, K., Carbone, C. & Kaiser, U. (2011). *Carbon*, **49**, 966–972.
- Pacilé, D., Papagno, M., Rodríguez, A. F., Grioni, M., Papagno, L., Girit, C. O., Meyer, J. C., Begtrup, G. E. & Zettl, A. (2008). *Phys. Rev. Lett.* **101**, 066806.
- Shin, H.-J. (2013). Personal communication.
- Smit, E. de, Swart, I., Creemer, J. F., Karunakaran, C., Bertwistle, D., Zandbergen, H. W., de Groot, F. M. F. D. & Weckhuysen, B. M. (2009). *Angew. Chem.* **121**, 3686–3690.
- Strachan, J. P., Pickett, M. D., Yang, J. J., Aloni, S., Kilcoyne, A. L. D., Medeiros-Ribeiro, G. & Stanley Williams, R. S. (2010). *Adv. Mater.* **22**, 3573–3577.
- Strachan, J. P., Strukov, D. B., Borghetti, J., Yang, J. J., Medeiros-Ribeiro, G. & Williams, R. S. (2011). *Nanotechnology*, **22**, 254015.
- Strachan, J. P., Yang, J. J., Münstermann, R., Scholl, A., Medeiros-Ribeiro, G., Stewart, D. R. & Stanley Williams, R. S. (2009). *Nanotechnology*, **20**, 485701.
- Takekoh, R., Okubo, M., Araki, T., StöVer, H. D. H. & Hitchcock, A. P. (2005). *Macromolecules*, **38**, 542–551.
- Yang, J. & Hu, G. (2012). *RSC Adv.* **2**, 11410.
- Yoon, T. H. (2009). *Appl. Spectrosc. Rev.* **44**, 2.
- Yoon, T. H., Benzerara, K., Ahn, S. W., Luthy, R. G., Tylliszczak, T. & Brown, G. E. Jr (2006). *Environ. Sci. Technol.* **40**, 5923–5929.
- Zelenay, V., Mooser, R., Tritscher, T., Křepelová, A., Heringa, M. F., Chirico, R., Prévôt, A. S. H., Weingartner, E., Baltensperger, U., Dommen, J., Watts, B., Raabe, J., Huthwelker, T. & Ammann, M. (2011). *Atmos. Chem. Phys.* **11**, 11777–11791.
- Zhou, J. G., Wang, J., Sun, C. L., Maley, J. M., Sammynaiken, R., Sham, T. K. & Pong, W. F. (2011). *J. Mater. Chem.* **21**, 14622.
- Zhou, J., Wang, J., Fang, H., Wu, C., Cutler, J. N. & Sham, T.-K. (2010a). *Chem. Commun.* **46**, 2778.
- Zhou, J., Wang, J., Liu, H., Banis, M. N., Sun, X. & Sham, T.-K. (2010b). *J. Phys. Chem. Lett.* **1**, 1709–1713.
- Zuckerman, J. J. & Hagen, A. P. (1990). *Inorganic Reactions and Methods*, Vol. 17, *Oligomerization and Polymerization Formation of Intercalation Compounds*. New York: Wiley-VCH.